Crystalline Control of {111} Bounded Pt_3Cu Nanocrystals: Multiply-Twinned Pt_3Cu Icosahedra with Enhanced Electrocatalytic Properties

Xiuhui Sun,[†] Kezhu Jiang,[†] Nan Zhang,[†] Shaojun Guo,[*,‡] and Xiaoqing Huang[*,†]

[†]College of Chemistry, Chemical Engineering and Materials Science, Soochow University, Jiangsu 215123, China and [‡]Physical Chemistry and Applied Spectroscopy, Los Alamos National Laboratory, Los Alamos, New Mexico 87545, United States

ABSTRACT Despite that different facets have distinct catalytic behavior, the important role of twin defects on enhancing the catalytic performance of metallic nanocrystals is largely unrevealed. The key challenge in demonstrating the importance of twin defects for catalysis is the extreme difficulties in creating nanostructures with the same exposed facets but tunable twin defects that are suitable for catalytic investigations. Herein, we show an efficient synthetic strategy to selectively synthesize {111}-terminated Pt_3Cu nanocrystals with controllable crystalline features. Two distinct {111}-bounded shapes, namely, multiply-twinned Pt_3Cu icosahedra and single-crystalline Pt_3Cu octahedra, are successfully prepared by simply changing the types of Cu precursors with the other growth parameters unchanged. Electrocatalytic studies show that the {111}-terminated Pt_3Cu nanocrystals exhibit the very interesting crystalline nature-dependent electrocatalytic activities toward both the oxygen reduction reaction (ORR) and methanol oxidation reaction (MOR) with multiply-twinned Pt_3Cu icosahedra demonstrating enhanced electrocatalytic activities compared to the single-crystalline Pt_3Cu octahedra due to their additional yet important effect of twin defect. As a result, under the multiple tuning conditions (alloy, shape, and twin effects), the multiply-twinned Pt_3Cu icosahedra exhibit much enhanced electrocatalytic activities in both ORR and MOR with respect to the Pt black. The present work highlights the importance of twin defects in enhancing electrocatalytic activities of metallic nanocrystals.

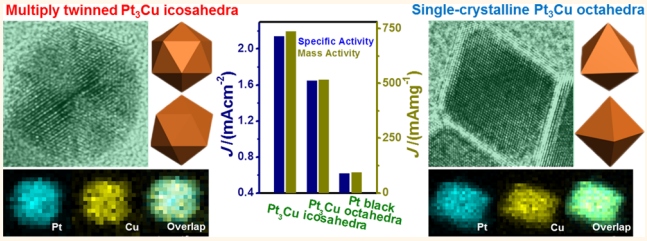

KEYWORDS: Platinum · copper · icosahedron · twin defect · electrocatalyst

The production of Pt-based nanocrystals with precise control over structures has continually attracted intensive research interest in the fields of physics and chemistry mainly due to their promising properties and various potential applications, including highly active catalysts in chemical conversions, sensors, and electrocatalysts in fuel cells.[1−9] It has been generally recognized that the catalytic behavior of metallic nanocrystals toward a specific catalytic process is highly dependent on their structures.[10,11] Following this guideline, multiple strategies have been developed to control the shapes of Pt-based nanocrystals with diverse compositions.[12−22] The well-defined Pt-based nanocrystals prepared so far are mainly dominated by shapes such as sphere, cube, octahedron, tetrahedron, and icosahedron.[12−30] The majority of previous strategies overwhelmingly focus on manipulating the exposed facets by choosing specific shape-directing agents.[12−30] Nevertheless, the ultimate catalytic property of the Pt-based nanocrystals is determined not only by its exposed facets but also by their interior crystalline nature, e.g., single-crystal vs twinned (single twinned, multiple twinned, etc.).[23,24] However, limited strategies are able to create Pt-based nanocrystals with controllable twin defects.[23,24]

In fact, twinning is a critical subject in the research field of material science and has been extensively studied in bulk materials or in substrates for many years.[31−33] The presence of twin defects in metallic materials has indeed a profound effect on their properties. However, the role of twin defects on the catalytic activities of metallic nanocrystals is much less explored because

* Address correspondence to hxq006@suda.edu.cn, shaojun.guo.nano@gmail.com.

Received for review May 17, 2015 and accepted July 8, 2015.

Published online July 14, 2015
10.1021/acsnano.5b02986

current synthetic strategies are hard to control the twin defects within the same exposed facets. Also, the twin effect is usually plagued with extensive composition effect and facet effect, which prevent a fundamental understanding of the exact role of the twin defects for optimized catalytic performance.[34−36]

Herein, we report an effective synthetic strategy for the preparation of well-defined Pt_3Cu nanocrystals in a controllable fashion. Two distinct {111}-bounded shapes, namely, multiply-twinned Pt_3Cu icosahedra and single-crystalline Pt_3Cu octahedra[27−30] have been selectively prepared by simply changing the types of Cu precursors with the other synthesis parameters unchanged. To the best of our knowledge, this is the first synthesis of well-defined PtCu icosahedra. A robust synthetic approach to the selective production of Pt_3Cu icosahedra and Pt_3Cu octahedra has not been achieved yet. Significantly, the successful creation of crystalline-controlled Pt_3Cu nanocrystals with identical exposed facets and same compositions provides an ideal platform for studying the effect of twin defects on catalysis. As a consequence, we found that the multiply-twinned Pt_3Cu icosahedra exhibited the improved electrocatalytic activities toward both the oxygen reduction reaction (ORR) and methanol oxidation reaction (MOR) relative to the single-crystalline Pt_3Cu octahedra because of their additional effect of twin defect, despite they are all bounded by the same {111} facets. Under the multiple tuning conditions (alloy, shape, and twin effects), the multiply-twinned Pt_3Cu icosahedra could show 5.58 and 12.71 times higher specific and mass activities for ORR, and 3.48 and 7.92 times higher specific and mass activities for MOR than commercial Pt black. The present work opens a new way for enhancing the electrocatalytic performance of metal nanocrystals through the introduction of unique twin defect.

RESULTS AND DISCUSSION

To prepare icosahedral Pt_3Cu nanocrystals, platinum(II) acetylacetonate ($Pt(acac)_2$), copper(II) chloride dihydrate ($CuCl_2 \cdot 2H_2O$), ascorbic acid (AA), and cetyltrimethylammonium bromide (CTABr) were dissolved in *N*,*N*-dimethylformamide (DMF) under magnetic stirring for around 0.5 h (see Experimental Section for details). The resulting homogeneous mixture was transferred to a Teflon-lined stainless-steel autoclave and then heated at 150 °C for 5 h before it was cooled to room temperature. The resulting colloidal nanocrystals were collected by centrifugation and washed three times with an ethanol/acetone mixture.

Detailed characterizations of as-prepared Pt_3Cu icosahedra are shown in Figure 1 and Figure S1. Typical transmission electron microscopy (TEM) (Figure 1a; Figure S1a−c) and high-angle annular dark-field scanning TEM (HAADF-STEM) images (Figure 1b; Figure S1d) show that the majority of the products

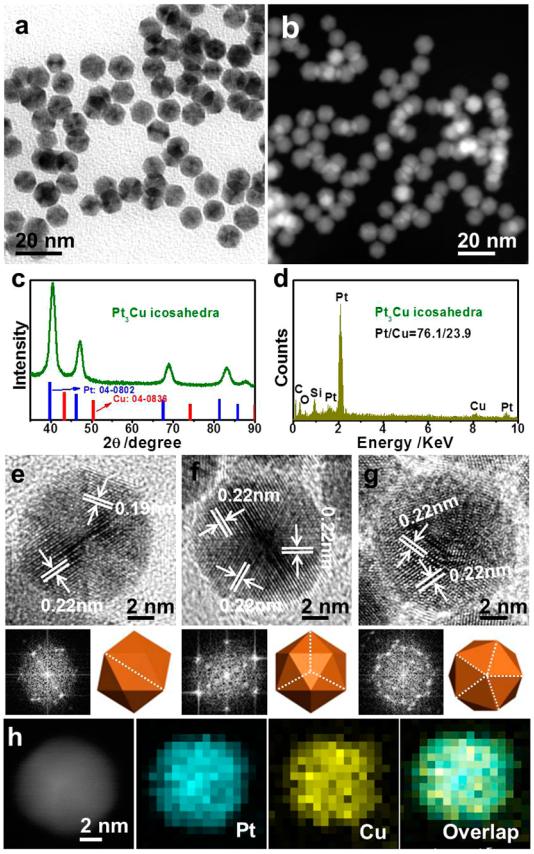

Figure 1. Representative (a) TEM and (b) HAADF-STEM, TEM images, (c) PXRD pattern, and (d) SEM-EDX of Pt_3Cu icosahedra. (e−g) HRTEM images, corresponding FFT images, and geometrical models of Pt_3Cu icosahedra oriented along three typical projections. (h) HAADF-STEM elemental mapping results for individual Pt_3Cu icosahedra.

have hexagonal profiles. The nanocrystals are monodisperse, with an average edge length of 5 ± 0.4 nm. The powder X-ray diffraction (PXRD) pattern of the nanocrystals shows a face-centered-cubic (*fcc*) structure with the peak positions in between Pt and Cu diffractions, respectively (Figure 1c), revealing the formation of alloyed structure of the Pt_3Cu nanocrystals. The Pt/Cu composition is around 3/1, as confirmed by both inductively coupled plasma atomic emission spectroscopy (ICP-AES, Table S1) and scanning electron microscopy-EDX (SEM-EDX) (Figure 1d). To further figure out the detailed structure of the obtained nanocrystals, high-resolution TEM (HRTEM) images of individual Pt_3Cu icosahedron were carefully collected (Figure 1e−g). The twin boundaries are clearly observed in all the characterized nanocrystals without exceptions. These typical images projected along the two-, three-, and five-fold axis collectively reveal that the as-grown nanocrystals are essential icosahedra, which matches well the geometric models of icosahedra consisting of 20 tetrahedral subunits with 30 twin boundaries and 20 exposed {111} triangle facets (Figure 1e−g).[37] The fast Fourier transforms (FFTs) of the Pt_3Cu icosahedra further confirms their

multiply-twinned structures.[23,24,38−40] The lattice spacings are measured to be 0.22 and 0.19 nm, corresponding to the {111} and {200} plane of *fcc* Pt_3Cu nanocrystals, respectively. The alloyed structure was also confirmed by the HAADF-STEM-energy-dispersive X-ray spectroscopy (HAADF-STEM-EDX) elemental mapping analysis, where the distribution of Pt and Cu are even through the whole icosahedron (Figure 1h).

To understand the growth mechanism of the Pt_3Cu icosahedra, we thoroughly investigated the experimental parameters on the morphologies of resulting nanocrystals. Among all the experimental parameters, CTABr introduced in our synthesis appears to be the key for the preparation of Pt_3Cu icosahedra. The reaction in the absence of CTABr cannot produce icosahedra. The products are made of severely aggregated nanostructures associated with octahedra (Figure S2a,b), indicating that the CTABr performs not only as surfactant but also shape-directing agent. To further explore whether CTA^+ or Br^- in CTABr is necessary in our synthesis, CTABr was replaced by cetyltrimethylammonium chloride (CTACl) and NaBr, respectively. As showed in Figure S3a,b, when CTABr was replaced with CTACl, the sample containing the mixture of icosahedra and octahedra was obtained. This might be ascribed to the weaker coordination ability of Cl^- than Br^-; in this case, the stabilization for high density of twin defects of icosahedra is insufficient. Therefore, icosahedral nanocrystals were obtained by replacing CTABr with NaBr (Figure S2c,d), despite that they are aggregated heavily. We thus conclude that Br^- other than CTA^+ promotes the growth of icosahedral nanocrystals, although CTA^+ is necessary for the dispersion of icosahedra. This conclusion was experimentally confirmed by the fact that typical icosahedra were prepared when CTABr was replaced by the combination of CTACl and NaBr (Figure S3c,d).

In addition to the critical role of CTABr, the selective use of AA and DMF was also important for the growth of Pt_3Cu icosahedra. For example, when glucose was introduced to replace AA, a mixture of icosahedra and octahedra was obtained (Figure S4a,b). If replacing DMF with 1-methyl-2-pyrrolidinone (NMP), another widely used solvent, and keeping all other experimental conditions the same, irregular nanocrystals rather than icosahedra were observed (Figure S4c,d). In the synthesis of PdCu icosahedra, we have also studied the effect of the Pt/Cu precursor ratios on the morphology and composition of the products. The results show that all the obtained nanocrystals have icosahedral shapes with similar edge lengths at around 5.0 nm (Figure S5a, b). The PXRD patterns of all the as-prepared icosahedra display similar peaks that can be indexed as *fcc* Pt_3Cu (Figure S5c). The composition of these obtained Pt_3Cu icosahedra were characterized by ICP-AES and SEM-EDX (Figure S5d). According to the analysis of SEM-EDX, $Pt_{76.1}Cu_{23.9}$, $Pt_{75.5}Cu_{24.5}$, and $Pt_{75.5}Cu_{24.5}$ were obtained when the molar ratio of $Pt(acac)_2$/$Cu(acac)_2$ were 2/2, 2/3, and 2/4, respectively. It is apparent that the feeding ratios of the Pt and Cu precursors had very limited influence on the compositions and the morphology of the Pt_3Cu icosahedra. This may be attributed to the difficulty in reducing Cu(II)/Cu in the current system and the strong tendency of Cu to alloy with Pt to form Pt_3Cu nanostructures, being similar to a case of synthesis of Pt_3Ni nanostructures.[41]

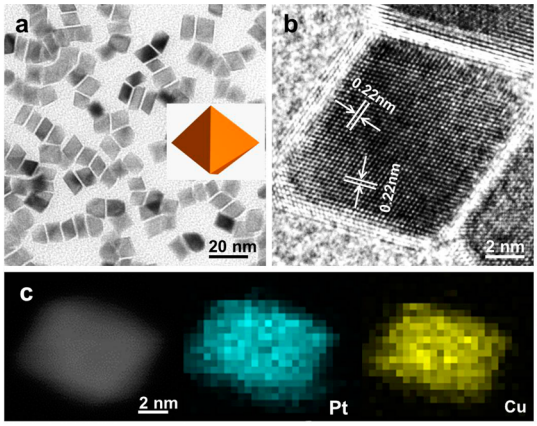

Figure 2. Representative (a) TEM, (b) HRTEM, and (c) HAADF-STEM elemental mapping images of Pt_3Cu octahedra. Inset in (a) shows a geometrical model of Pt_3Cu octahedron.

Interestingly, when we simply switched Cu precursor from $CuCl_2$ to $Cu(acac)_2$ with other parameters identical to the synthesis of Pt_3Cu icosahedra, the well-defined Pt_3Cu octahedra were generated (Figure 2). As shown in Figure 2a and Figure S6a,b, the Pt_3Cu octahedra have an edge length of 7.5 ± 1 nm. The HRTEM image (Figure 2b) of an individual Pt_3Cu octahedron shows clear lattice fringes with an interfringe lattice of around 0.22 nm, corresponding to the lattice spacing of the Pt_3Cu {111} plane. The PXRD pattern (Figure S6c) of the Pt_3Cu octahedra reveals an *fcc* structure with no detectable peaks from either Pt or Cu nanostructures, confirming the formation of alloyed structure of Pt_3Cu nanocrystals. The elemental distributions of Pt and Cu were further revealed by the HAADF-STEM-EDX elemental mapping on an individual Pt_3Cu octahedron (Figure 2c). The result shows the complete overlapping of two metal components, confirming the formation of alloyed structure. The SEM-EDX and ICP-AES results suggest a molar ratio of 3/1 (Pt/Cu) of the Pt_3Cu octahedra (Figure S6d).

The as-made Pt_3Cu icosahedra and Pt_3Cu octahedra, with the same exposed {111} facets but different crystalline nature are ideal model nanocrystals for investigating whether the high density of twin defects can potentially offer the enhanced catalytic performance. To this end, we first chose ORR to evaluate the catalytic activities of the Pt_3Cu icosahedra and Pt_3Cu octahedra, and further benchmarked against the commercial Pt black catalyst (Aldrich, 205915-1G, ≥99.97%, Figure S7). The electrocatalytic property was

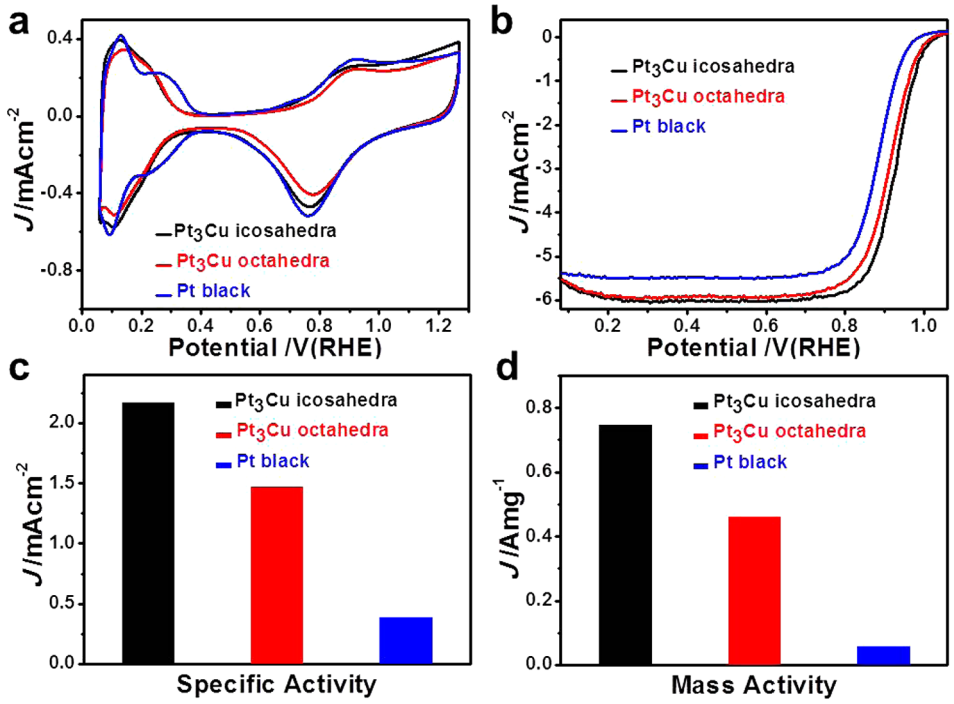

Figure 3. (a) CVs recorded at room temperature in 0.1 M $HClO_4$ solution with a sweep rate of 50 mV s^{-1}. (b) ORR polarization curves recorded at room temperature in an O_2-saturated 0.1 M $HClO_4$ aqueous solution with a sweep rate of 10 mV s^{-1} and a rotation rate of 1600 rpm. (c,d) Specific activity and mass activity at 0.9 V versus RHE for these three catalysts.

first investigated by using cyclic voltammetry (CV) recorded at room temperature in 0.1 M $HClO_4$ solution at a sweep rate of 50 mV s^{-1}. According to the CV curves shown in Figure 3a, the electrochemical surface areas (ECSAs) were calculated as 34.4 m^2 g^{-1} for Pt_3Cu icosahedra, 31.5 m^2 g^{-1} for Pt_3Cu octahedra, and 15.1 m^2 g^{-1} for Pt black. Figure 3b shows the ORR polarization curves of Pt_3Cu icosahedra, Pt_3Cu octahedra, and Pt black carried out in an oxygen-saturated 0.1 M $HClO_4$ solution at a sweep rate of 10 mV s^{-1} and at a rotation rate of 1600 rpm by using the rotating disk electrode (RDE). From the polarization curves, the calculated kinetic current density at 0.9 V was then normalized over the Pt loading weight and ECSA to give the mass activity and specific activity, respectively (Figure 3c,d). We find that the catalytic specific and mass activities follow the order of Pt_3Cu icosahedra > Pt_3Cu octahedra > Pt black. Interestingly, the Pt_3Cu icosahedra showed a specific activity of 2.17 mA cm^{-2} and mass activity of 0.746 A mg^{-1}, a 47.6% specific activity and 61.8% mass activity enhancement compared with the Pt octahedra (1.47 mA cm^{-2} and 0.461 mA mg^{-1}), despite the fact that both shapes are bounded by {111} facets.

We also evaluated the electrocatalytic activities of the Pt_3Cu nanocrystals for MOR. In the forward scan, the peak potential of Pt_3Cu icosahedra (1.00 V) is lower than that of Pt_3Cu octahedra (1.08 V) (Figure 4a), indicating the higher electrocatalytic activity of Pt_3Cu icosahedra. The peak current of different catalysts was normalized over the Pt loading weight and ECSA to give the mass activity and specific activity, respectively. The mass and specific activities of all catalysts for MOR are summarized in Figure 4b in which the Pt_3Cu icosahedra exhibit the highest mass activity and specific activity. The mass activity of Pt_3Cu icosahedra is measured to be 736 mA mg^{-1}, which is 1.42 times and 7.92 times higher than those of the Pt_3Cu octahedra and Pt black, respectively (Figure 4b). Similarly, the maximum specific activity of the Pt_3Cu icosahedra was 2.14 mA cm^{-2}, 1.31 times and 3.48 times higher than those of the Pt_3Cu octahedra and Pt black, respectively (Figure 4b). The durability of the Pt_3Cu icosahedra, Pt_3Cu octahedra, and commercial Pt black was also tested by repeating the CV sweeps for 400 cycles (Figure S8). After 400 sweeping cycles, 85.7% of the initial catalytic activity was still maintained for the Pt_3Cu icosahedra, as compared with the loss of 28.1% for Pt_3Cu octahedra and 27.5% for Pt black, suggesting that the Pt_3Cu icosahedra had a better durability than those of the Pt_3Cu octahedra and Pt black. These Pt_3Cu polyhedra after the durability tests were scratched off the electrode and collected by sonication for fur ther TEM/HRTEM/STEM mapping characterizations. As shown in Figures S9 and S10, these Pt_3Cu polyhedra largely preserved their morphologies and compositions, showing a good structure stability of the obtained Pt_3Cu polyhedra.

Considering that the Pt_3Cu icosahedra have the same exposed {111} facets and composition as the Pt_3Cu octahedra, the observation of the improved intrinsic electrocatalytic activities of Pt_3Cu icosahedra

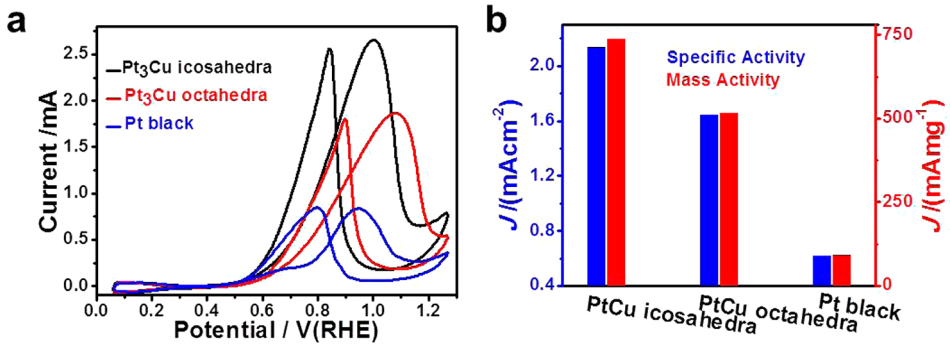

Figure 4. (a) CVs recorded at room temperature in the mixture of 0.1 M $HClO_4$ and 0.2 M CH_3OH solution with a sweep rate of 50 mV s^{-1}. (b) Specific and mass activities of the three catalysts.

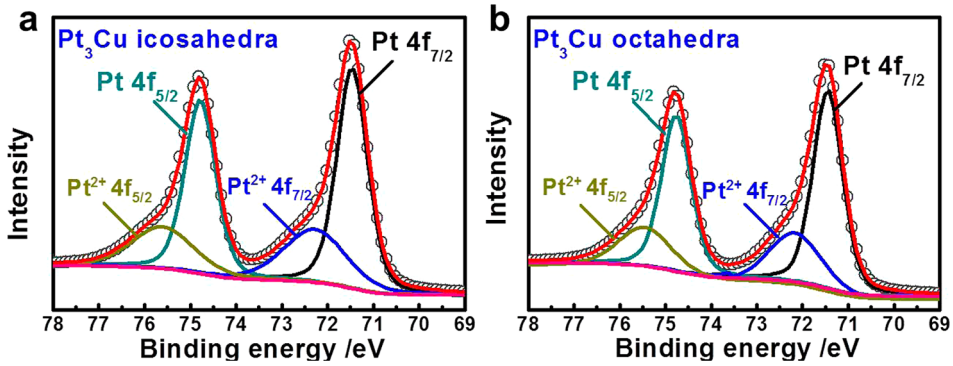

Figure 5. Pt XPS spectra of (a) Pt_3Cu icosahedra and (b) Pt_3Cu ocatahedra. The Pt XPS spectra of both Pt_3Cu icosahedra and Pt_3Cu octahedra show two peaks that can be assigned to Pt $4f_{7/2}$ and Pt $4f_{5/2}$ states, and each state can be further split into two doublets, associated with Pt^0 (black curves) and Pt^{2+} (blue curves) chemical states. The integrated area of Pt^{2+} in Pt 4f7/2 is divided by the integrated area of Pt 4f7/2 to generate the Pt^{2+} fractions in both Pt_3Cu icosahedra and Pt_3Cu octahedra.

for both ORR and MOR is particularly obvious, strongly indicating that twin defects play a critical role in further enhancing the catalytic activity for both the ORR and MOR.[23,24] We propose that the presence of structural defects like twin boundaries in Pt_3Cu icosahedra will lead to more dangling bonds and increase the number of free Pt sites on the surface, which leads to a more active heterogeneous catalyst.

We conducted X-ray photoelectron spectroscopy (XPS) analysis to determine the chemical states of the Pt_3Cu icosahedra and Pt_3Cu octahedra catalysts. In general, XPS Pt spectra of Pt_3Cu nanocrystals show two peaks that can be assigned to Pt $4f_{7/2}$ and Pt $4f_{5/2}$ states and can be further split into two doublets, associated with Pt^0 and Pt^{2+} chemical states (Figure 5). It is calculated that the Pt^{2+} fraction in Pt_3Cu icosahedra (26.8%) is higher than that of Pt_3Cu octahedra (20.1%), being consistent with the fact that the increased number of free Pt sites on the surface of icosahedra can improve the possibility of being oxidized. Based on previous study on the bulk surface, the kinetics of O_2 reduction are determined by the number of free Pt sites available for the adsorption of O_2 and by the Gibbs energy of adsorption of O_2 and intermediates.[42] Given that the exposed facets and compositions of the Pt_3Cu icosahedra and Pt_3Cu octahedra are identical, the Gibbs energy of adsorption of O_2 and intermediates in the Pt_3Cu nanocrystals can be the similar. Therefore, one of the key parameters that determines the enhanced ORR activity of Pt_3Cu icosahedra should be their increased number of free Pt adsorption sites (additionally come from twin defect) available for the O_2. It was also previously suggested that the structural defects could serve as possible channels for O_2 incorporation.[43] When O_2 is incorporated into the nanocrystals through the defect boundaries, the interaction between oxygen and the electron cloud of the adjacent Pt atoms can positively shift the chemical state of Pt atoms and activate O_2 for the subsequent oxidation reaction. Therefore, the presence of twin defects in Pt_3Cu icosahedra can provide better opportunity for the adsorption, activation, and dissociation of small fuel cell molecules, and result in an enhanced catalytic property.[43]

CONCLUSIONS

In summary, we have developed a facile wet chemical strategy that allows the selective creation of {111}-terminated Pt_3Cu nanocrystals with a controllable fashion. Two distinct Pt_3Cu nanocrystals, namely, icosahedral and octahedral nanocrystals, can be selectively prepared. To the best of our knowledge, this is the first example that unique Pt_3Cu icosahedra can be prepared with high yield. In the developed strategy, the CTA^+ functions as surfactant to disperse the

colloid, while the Br^- functions as the shape-directing agent to induce the growth of Pt_3Cu icosahedra with high density of twin defects. Because of their high density of twin defects and high lattice strains, these multiply-twinned Pt_3Cu icosahedra exhibit enhanced electrocatalytic activities toward both ORR and MOR relative to single-crystalline Pt_3Cu octahedra, despite that they have the same exposed facets and compositions. We expect this fundamental research will inspire new rational design of Pt-based catalysts with further enhanced performance for fuel cell reactions, various chemical conversions, and beyond.

EXPERIMENTAL SECTION

Chemicals. Platinum(II) acetylacetonate ($Pt(acac)_2$, 97%), copper(II) acetylacetonate ($Cu(acac)_2$, 97%), ascorbic acid ($C_6H_8O_6$, AA, reagent grade), cetyltrimethylammonium bromide (CTABr, AR), cetyltrimethylammonium chloride (CTACl, AR), and 1-methyl-2-pyrrolidinone (C_5H_9NO, NMP, 99%) were all purchased from Sigma-Aldrich. Copper(II) chloride dihydrate ($CuCl_2 \cdot 2H_2O$, reagent grade), *N*,*N*-dimethylformamide (C_3H_7NO, DMF, 99%), glucose ($C_6H_{12}O_6$, reagent grade), and sodium bromide (NaBr, reagent grade) were purchased from Sinopharm Chemical Reagent Co. Ltd. (Shanghai, China). All the chemicals were used as received without further purification. The water (18 MΩ/cm) used in all experiments was prepared by passing through an ultrapure purification system (Aqua Solutions).

Preparation of Pt_3Cu Icosahedra and Pt_3Cu Octhaedra. In a typical preparation of Pt_3Cu icosahedra, platinum(II) acetylacetonate ($Pt(acac)_2$, 10.0 mg), copper(II) chloride dihydrate ($CuCl_2 \cdot 2H_2O$, 4.2 mg), cetyltrimethylammonium bromide (CTABr, 36.5 mg), and ascorbic acid (AA, 35.6 mg) were mixed with *N*,*N*-dimethylformamide (DMF, 10.0 mL) under magnetic stirring for about 0.5 h. The resulting homogeneous mixture was transferred to a Teflon-lined stainless-steel autoclave and then heated at 150 °C for 5 h, before it was cooled to room temperature. The resulting products were collected by centrifugation and washed with an ethanol/acetone mixture for three times. The synthesis of Pt_3Cu octahedra was similar to that of Pt_3Cu icosahedra, except that $CuCl_2$ was replaced by equal moles of $Cu(acac)_2$.

Characterizations. TEM, STEM, HAADF-STEM-EDX were conducted on an FEI Tecnai F20 transmission electron microscope at an acceleration voltage of 200 kV. Scanning electron microscopy (SEM) characterizations were taken at 5 kV by using Supra 55 from Carl Zeiss. The samples were prepared by dropping ethanol dispersion of samples onto carbon-coated copper TEM grids (for TEM images) or nickel TEM grids (for STEM elemental mappings) using pipettes and dried under ambient conditions. The samples, after the electrochemical tests, were scratched off the electrode and collected by sonication for further TEM/HRTEM/STEM mapping characterizations. X-ray photoelectron spectra (XPS) were collected with an SSI S-Probe XPS Spectrometer. Powder X-ray diffraction (PXRD) patterns were collected on a Shimadzu XRD-6000 X-ray diffractometer. The concentration of catalysts was determined by the inductively coupled plasma atomic emission spectroscopy (710-ES, Varian, ICP-AES).

Elecrocatalytic Measurements. For the ORR measurements, a typical three-electrode cell was used to perform the electrochemical measurements. The working electrode was a glassy-carbon rotating disk electrode (RDE) (diameter, 5 mm; area, 0.196 cm^2) from the Pine Instrument. Ag/AgCl (3 M KCl) and Pt rod were used as reference and counter electrode. To prepare the working electrode, the Pt_3Cu nanocrystals were mixed with ethanol, water, and Nafion (5%) (v/v/v = 9:1:0.02) and sonicated for 5 min to form a catalyst ink. The concentration of metal Pt was controlled to be 0.36 mg/mL based on ICP-AES measurement. Ten microliters of the catalyst ink was cast on an RDE and dried under ambient conditions. The loading amount of metal Pt for the Pt_3Cu nanocrystals catalyst was 3.6 μg. The ECSAs were determined by integrating the hydrogen adsorption charge on the CV at room temperature in nitrogen-saturated 0.1 M $HClO_4$ solution. The potential scan rate was 50 mV s^{-1} for the CV measurement. ORR measurements were conducted in a 0.1 M $HClO_4$ solution purged with oxygen during the measurement. The scan rate and rotation rate for ORR measurement were 10 mV s^{-1} and 1600 rpm. For comparison, the commercial Pt black was used as the benchmark catalyst with a loading amount of 9 μg. For the MOR measurements, a 10 μL ethanol dispersion of Pt_3Cu icosahedra (0.36 mg_{Pt}/mL) or Pt_3Cu octahedra (0.36 mg_{Pt}/mL) was deposited on a glassy carbon electrode to obtain the working electrodes after the solvent is dried naturally. Nafion was not used in the preparation of the catalyst link. MOR measurements were conducted in a 0.1 M $HClO_4$ + 0.2 M CH_3OH solution in the stationary condition. The scan rate for methanol electrooxidation was 50 mV s^{-1}.

Conflict of Interest: The authors declare no competing financial interest.

Supporting Information Available: Figure S1−10. The Supporting Information is available free of charge on the ACS Publications website at DOI: 10.1021/acsnano.5b02986.

Acknowledgment. This work was financially supported by the start-up funding from Soochow University and Young Thousand Talented Program.

REFERENCES AND NOTES

1. Chen, A. C.; Holt-Hindle, P. Platinum-Based Nanostructured Materials: Synthesis, Properties, and Applications. *Chem. Rev.* **2010**, *110*, 3767.
2. Wu, J.; Yang, H. Platinum-Based Oxygen Reduction Electrocatalysts. *Acc. Chem. Res.* **2013**, *46*, 1848.
3. Zhang, H.; Jin, M.; Xia, Y. Enhancing the Catalytic and Electrocatalytic Properties of Pt-based Catalysts by Forming Bimetallic Nanocrystals with Pd. *Chem. Soc. Rev.* **2012**, *41*, 8035.
4. Guo, S. J.; Zhang, S.; Sun, S. H. Tuning Nanoparticle Catalysis for the Oxygen Reduction Reaction. *Angew. Chem., Int. Ed.* **2013**, *52*, 8526.
5. Tian, N.; Zhou, Z. Y.; Sun, S. G.; Ding, Y.; Wang, Z. L. Synthesis of Tetrahexahedral Platinum Nanocrystals with High-Index Facets and High Electro-Oxidation Activity. *Science* **2007**, *316*, 732.
6. Lim, B.; Jiang, M. J.; Camargo, P. H. C.; Cho, E. C.; Tao, J.; Lu, X. M.; Zhu, Y. M.; Xia, Y. N. Pd-Pt Bimetallic Nanodendrites with High Activity for Oxygen Reduction. *Science* **2009**, *324*, 1302.
7. Yamada, Y.; Tsung, C. K.; Huang, W.; Huo, Z. Y.; Habas, S. E.; Soejima, T.; Aliaga, C. E.; Somorjai, G. A.; Yang, P. D. Nanocrystal Bilayer for Tandem Catalysis. *Nat. Chem.* **2011**, *3*, 372.
8. Wang, D.; Xin, H. L.; Hovden, R.; Wang, H.; Yu, Y.; Muller, D. A.; DiSalvo, F. J.; Abruña, H. D. Structurally Ordered Intermetallic Platinum-Cobalt Core-Shell Nanoparticles with Enhanced Activity and Stability as Oxygen Reduction Electrocatalysts. *Nat. Mater.* **2013**, *12*, 81.
9. Gasteiger, H. A.; Markovi, N. M. Just a Dream-or Future Reality? *Science* **2009**, *324*, 48.
10. Wang, Z. L. Transmission Electron Microscopy of Shape-Controlled Nanocrystals and Their Assemblies. *J. Phys. Chem. B* **2000**, *104*, 1153.
11. Tian, N.; Zhou, Z. Y.; Sun, S. G. Platinum Metal Catalysts of High-Index Surfaces: From Single-Crystal Planes to Electrochemically Shape-Controlled Nanoparticles. *J. Phys. Chem. C* **2008**, *112*, 19801.
12. Chen, C.; Kang, Y.; Huo, Z.; Zhu, Z.; Huang, W.; Xin, H. L.; Snyder, J. D.; Li, D.; Herron, J. A.; Mavrikakis; et al.

Highly Crystalline Multimetallic Nanoframes with Three-Dimensional Electrocatalytic Surfaces. *Science* **2014**, *343*, 1339.
13. Cui, C.; Gan, L.; Heggen, M.; Rudi, S.; Strasser, P. Compositional Segregation in Shaped Pt Alloy Nanoparticles and Their Structural Behaviour During Electrocatalysis. *Nat. Mater.* **2013**, *12*, 765.
14. Habas, S. E.; Lee, H.; Radmilovic, V.; Somorjai, G. A.; Yang, P. D. Shaping Binary Metal Nanocrystals Through Epitaxial Seeded Growth. *Nat. Mater.* **2007**, *6*, 692.
15. Wu, J. B.; Gross, A.; Yang, H. Shape and Composition-Controlled Platinum Alloy Nanocrystals Using Carbon Monoxide as Reducing Agent. *Nano Lett.* **2011**, *11*, 798.
16. Zhang, J.; Fang, J. Y. A General Strategy for Preparation of Pt 3d-Transition Metal (Co, Fe, Ni) Nanocubes. *J. Am. Chem. Soc.* **2009**, *131*, 18543.
17. Kang, Y. J.; Murray, C. B. Synthesis and Electrocatalytic Properties of Cubic Mn-Pt Nanocrystals (Nanocubes). *J. Am. Chem. Soc.* **2010**, *132*, 7568.
18. Xu, D.; Liu, Z. P.; Yang, H. Z.; Liu, Q. S.; Zhang, J.; Fang, J. Y.; Zou, S. Z.; Sun, K. Solution-Based Evolution and Enhanced Methanol Oxidation Activity of Monodisperse Platinum-Copper Nanocubes. *Angew. Chem., Int. Ed.* **2009**, *48*, 4217.
19. Chen, J. Y.; Wiley, B.; McLellan, J.; Xiong, Y. J.; Li, Z. Y.; Xia, Y. N. Optical Properties of Pd-Ag and Pt-Ag Nanoboxes Synthesized *via* Galvanic Replacement Reactions. *Nano Lett.* **2005**, *5*, 2058.
20. Zhang, J.; Yang, H. Z.; Fang, J. Y.; Zou, S. Z. Synthesis and Oxygen Reduction Activity of Shape-Controlled Pt_3Ni Nanopolyhedra. *Nano Lett.* **2010**, *10*, 638.
21. Wu, J. B.; Zhang, J. L.; Peng, Z. M.; Yang, S. C.; Wagner, F. T.; Yang, H. Truncated Octahedral Pt_3Ni Oxygen Reduction Reaction Electrocatalysts. *J. Am. Chem. Soc.* **2010**, *132*, 4984.
22. Wu, Y. E.; Cai, S. F.; Wang, D. S.; He, W.; Li, Y. D. Syntheses of Water-Soluble Octahedral, Truncated Octahedral, and Cubic Pt-Ni Nanocrystals and Their Structure-Activity Study in Model Hydrogenation Reactions. *J. Am. Chem. Soc.* **2012**, *134*, 8975.
23. Wu, J.; Qi, L.; You, H.; Gross, A.; Li, J.; Yang, H. Icosahedral Platinum Alloy Nanocrystals with Enhanced Electrocatalytic Activities. *J. Am. Chem. Soc.* **2012**, *134*, 11880.
24. Zhou, W.; Wu, J.; Yang, H. Highly Uniform Platinum Icosahedra Made by Hot Injection-Assisted GRAILS Method. *Nano Lett.* **2013**, *13*, 2870.
25. Wang, M.; Zhang, W.; Wang, J.; Minett, A.; Lo, V.; Liu, H.; Chen, J. Mesoporous Hollow PtCu Nanoparticles for Electrocatalytic Oxygen Reduction Reaction. *J. Mater. Chem. A* **2013**, *1*, 2391.
26. Marcu, A.; Toth, G.; Srivastava, R.; Strasser, P. Preparation, Characterization and Degradation Mechanisms of PtCu Alloy Nanoparticles for Automotive Fuel Cells. *J. Power Sources* **2012**, *208*, 288.
27. Jia, Y.; Su, J.; Chen, Z.; Tan, K.; Chen, Q.; Cao, Z.; Jiang, Y.; Xie, Z.; Zheng, L. Composition-Tunable Synthesis of Pt-Cu Octahedral Alloy Nanocrystals from PtCu to $PtCu_3$ *via* Underpotential-Deposition-Like Process and Their Electro-Catalytic Properties. *RSC Adv.* **2015**, *5*, 18153.
28. Jiang, Y.; Jia, Y.; Zhang, J.; Zhang, L.; Huang, H.; Xie, Z.; Zheng, L. Underpotential Deposition-Induced Synthesis of Composition-Tunable Pt-Cu Nanocrystals and Their Catalytic Properties. *Chem. - Eur. J.* **2013**, *19*, 3119.
29. LaGrow, A. P.; Knudsen, K. R.; AlYami, N. M.; Anjum, D. H.; Bakr, O. M. Effect of Precursor Ligands and Oxidation State in the Synthesis of Bimetallic Nano-Alloys. *Chem. Mater.* **2015**, *27*, 4134.
30. Zhang, J.; Yang, H.; Martens, B.; Luo, Z.; Xu, D.; Wang, Y.; Zou, S.; Fang, J. Pt-Cu Nanoctahedra: Synthesis and Comparative Study with Nanocubes on Their Electrochemical Catalytic Performance. *Chem. Sci.* **2012**, *3*, 3302.
31. Wang, Y. M.; Chen, M. W.; Zhou, F. H.; Ma, E. High Tensile Ductility in a Nanostructured Metal. *Nature* **2002**, *419*, 912.
32. Chen, K. C.; Wu, W. W.; Liao, C. N.; Chen, L. J.; Tu, K. N. Observation of Atomic Diffusion at Twin-Modified Grain Boundaries in Copper. *Science* **2008**, *321*, 1066.
33. Algra, R. E.; Verheijen, M. A.; Borgstrom, M. T.; Feiner, L. F.; Immink, G.; van Enckevort, W. J. P.; Vlieg, E.; Bakkers, E. P. A. M. Twinning Superlattices in Indium Phosphide Nanowires. *Nature* **2008**, *456*, 369.
34. Bucur, R. V.; Indrea, E. Influence of the Crystalline Microstructure on the Diffusivity of Hydrogen in Palladium Galvanostatic Permeation and X-Ray-Diffraction Measurements. *Acta Metall.* **1987**, *35*, 1325.
35. Maier, J. Defect Chemistry: Composition, Transport, and Reactions in the Solid State; Part I: Thermodynamics. *Angew. Chem., Int. Ed. Engl.* **1993**, *32*, 313.
36. Maier, J. Defect Chemistry: Composition, Transport, and Reactions in the Solid State; Part II: Kinetics. *Angew. Chem., Int. Ed. Engl.* **1993**, *32*, 528.
37. Reyes-Gasga, J.; Tehuacanero-Nunez, S.; Montejano-Carrizales, J. M.; Gao, X. X.; Jose-Yacaman, J. M. Analysis of the Contrast in Icosahedral Gold Nanoparticles. *Top. Catal.* **2007**, *46*, 23.
38. Kang, Y.; Pyo, J. B.; Ye, X.; Diaz, R. E.; Gordon, T. R.; Stach, E. A.; Murray, C. B. Shape-Controlled Synthesis of Pt Nanocrystals: The Role of Metal Carbonyls. *ACS Nano* **2013**, *7*, 645.
39. Niu, Z. Q.; Peng, Q.; Gong, M.; Rong, H. P.; Li, Y. D. Oleylamine-Mediated Shape Evolution of Palladium Nanocrystals. *Angew. Chem., Int. Ed.* **2011**, *50*, 6315.
40. You, H.; Yang, S.; Ding, B.; Yang, H. Synthesis of Colloidal Metal and Metal Alloy Nanoparticles for Electrochemical Energy Applications. *Chem. Soc. Rev.* **2013**, *42*, 2880.
41. Huang, X. Q.; Zhu, E. B.; Chen, Y.; Li, Y. J.; Chiu, C. Y.; Xu, Y. X.; Lin, Z. Y.; Duan, X. F.; Huang, Y. A Facile Strategy to Pt_3Ni Nanocrystals with Highly Porous Features as an Enhanced Oxygen Reduction Reaction Catalyst. *Adv. Mater.* **2013**, *25*, 2974.
42. Stamenkovic, V. R.; Fowler, B.; Mun, B. S.; Wang, G.; Ross, P. N.; Lucas, C. A.; Markovic, N. M. Improved Oxygen Reduction Activity on $Pt_3Ni(111)$ *via* Increased Surface Site Availability. *Science* **2007**, *315*, 493.
43. Blume, R.; Niehus, H.; Conrad, H.; Bottcher, A. Surface-Defect-Mediated Channel for Oxygen Incorporation into Ru(0001). *J. Phys. Chem. B* **2004**, *108*, 14332.